Molecular level understanding of the free energy landscape in early stages of MOF nucleation.

Loukas Kollias[1], David C. Cantu[2,3], Marcus A. Tubbs[2], Roger Rousseau[2], Vassiliki-Alexandra Glezakou[2*], Matteo Salvalaglio[1*]

[1]Thomas Young Centre and Department of Chemical Engineering, University College London, London WC1E 7JE, UK; [2]Basic and Applied Molecular Foundations, Pacific Northwest National Laboratory, Richland WA, 99352 USA; [3]Chemical and Materials Engineering Department, University of Nevada, Reno, Reno NV, 89557 USA

KEYWORDS: Metal-Organic Frameworks, Nucleation, Molecular Dynamics, Well-Tempered Metadynamics.

ABSTRACT: The assembly mechanism of hierarchical materials controlled by the choice of solvent and presence of spectator ions. In this paper, we use enhanced sampling molecular dynamics methods to investigate these effects on the configurational landscape of metal-linker interactions in the early stages of synthesis, using MIL-101(Cr) as a prototypical example. Microsecond-long well-tempered metadynamics (WTmetaD) simulations uncover a complex free energy structural landscape, with distinct crystal (C) and non-crystal (NC) like configurations and their equilibrium population. In presence of ions (Na+, F-), we observe a complex effect on the crystallinity of secondary building units (SBUs), by encouraging/suppressing salt bridges between C configurations and consequently controlling the percentage of defects. Solvent effects are assessed by introducing N, N dimethylformamide (DMF) instead of water, where SBU adducts are appreciably more stable and compact. These results shed light on how solvent and ionic strength impact the free energy of assembly phenomena that ultimately control materials synthesis and defect formation.

INTRODUCTION

Tunable materials offer numerous possibilities for synthesis leading to desirable attributes like high porosity, surface area and separations capability. Porous materials of this kind include metal-organic frameworks (MOFs) that attract increasing interest due to their potential applicability in numerous industrial processes that include CO_2 capture and sequestration[1-3] to reduce environmental pollution, CH_4 storage[4-5] for natural gas applications, catalysis[6-7], drug delivery[8-9], separations[10-11] and water production from the air in dry climates[12]. MOF properties can be significantly changed upon the presence of defects; for example, defects are known to deteriorate mechanical stability[13-14], or they can offer novel ways of functionalization, without loss of stability[15]. Understanding the formation of defects during MOF synthesis is essential[16] to devising strategies that reduce their occurrence.

In recent years, MOF synthesis research has focused on material discovery by employing various experimental techniques to develop new MOFs. Nevertheless, a thorough investigation involves understanding of the mechanism of synthesis that takes place. In this respect, theoretical models should be validated with experimental findings. Molecular simulations intrinsically can access atomic level information and provide mechanistic details that are not always possible to identify from experimental studies. In this work, we provide insights into MOF synthesis by assessing interactions between its building blocks during the early stages of nucleation through molecular simulations. Furthermore, we investigate solvent and ionic effects on these interactions in order to elucidate their role in MOF assembly.

Due to the metal cations in MOFs, their synthesis is regularly carried out in presence of counterions. Therefore, studying the effect that ionic strength has in this process is meaningful in the modelling of MOF synthesis. More precisely, metal precursors are introduced in the form of metal nitrate hydrates (e.g. $Cr(NO_3)_3 \cdot 9H_2O$ in the case of chromium)[17] and fluoride has been used by experimentalists in the synthesis of MIL-101 (Cr) as it promotes rapid crystal growth of the material[18-19]. Fluoride anions have an affinity to the chromium at the metal center of MOF building units and their interaction assists the stability of the crystal structure[20]. Nevertheless, recent studies[21-24] have used alternative synthetic methods by replacing fluoride with hydroxide anions using deionized water[21-23].

In this work, the self-assembly of MIL-101 (Cr) SBU from its constituent half-SBUs is studied as a prototypical example to highlight the most important stages of nucleation. Existing data on synthesis kinetics[25] allow for validation of our model. The half-SBUs used in this research work are structural isomers of the MIL-101 (Cr) half structural building unit (half-SBU). These have been found to be relevant in the study by Cantu et al.[26], where they emerge from minimum energy pathways in the formation of a MIL-101 (Cr) SBU. Our hypothesis is that nucleation of the MOF lattice is the result of the assembly of these half-SBUs. MIL-101 half-SBUs are comprised of the tri-metal center with three coordinatively bound organic linkers, and three "open" sites for other half-SBUs to assemble with each other toward nucleation. More generally, half-SBUs are uncharged species with formed metal centers and an equal number of open and occupied linker sites. In situ spectroscopy and NMR studies provide concrete evidence that supports the hypothesis that nucleation proceeds by the formation and assembly of half-SBUs[27-29]. Overall, MOF formation is widely believed to follow a nucleation and crystal growth mechanism subject to configuration complexity of half-SBUs. Our aim in this work is to sample the configurational space of SBUs resulting from the dimerization of half-SBUs and calculate the distribution of their conformational variants at equilibrium. With this analysis, we ultimately assess the development of defects in the early stages of MOF crystallization.

Several (48 in total) microsecond-long MD simulations with enhanced sampling have been conducted. The overall number of emerging possible SBU configurations (around 300) demonstrates the complexity of the process and the need for extensive sampling. Furthermore, the addition of an increasing number

of ions to the system allows to uncover the role of solution composition in the formation of SBUs, and the probability of creating defective units from pair-wise half-SBU interactions.

METHODS

Chemical structures were visualized with VMD[30]. In the following sections, we present the methodology applied to carry out molecular simulations and processing of the data to compute equilibrium distributions.

Force fields

To achieve an extensive sampling of conformational isomers of both half-SBUs and SBUs in explicit solution, we resorted to a classical representation of molecular interactions. In all simulations we used the OPLS-AA force field[31] to model interactions in the terephthalate linkers. We complement the latter by tailoring the pair-wise interactions between chromium atoms and linkers using a Lennard-Jones potential following the work of Cantu et al.[26]. The overall procedure is presented in the SI, section IV. Regarding the bonded interactions, all bonds and angles involving Cr are constrained at their equilibrium values based on SBU structures optimized with density functional theory (DFT). Dihedral angles, instead, are estimated from geometry optimizations of the isolated metal center. All DFT data has been obtained from Cantu et al.[26] All simulations have been carried out in explicit solvent. We investigate both aqueous and N, N-dimethylformamide (DMF) solutions, with the explicit inclusion of counterions (Na^+, F^-). Water is simulated with the TIP3P model[32], while DMF and the ionic species are modelled using OPLS-AA[31] parameters. In the case of counterions, we use the standard GROMACS[33] parameters for OPLS-AA[31]. The initial structures and force field parameters for DMF are obtained from the chemical database available through the work of Caleman et al.[34] and van der Spoel et al.[35].

Conformational sampling with well-tempered metadynamics

Well-tempered metadynamics (WTmetaD)[36] was used to extensively characterize the conformational space of both half-SBUs and their dimers (SBUs). In all simulations, temperature and pressure conditions are maintained constant (298 K and 1 bar) by using the velocity rescale thermostat[37] and the Berendsen barostat[38], respectively. The cut-off for non-bonded interactions is 10 Å. Long range electrostatic interactions were treated using a particle-mesh Ewald scheme[39]. Dynamics were propagated with a leapfrog integrator using a time step of 2 fs, while constraining bond lengths using LINCS[40]. A cubic simulation box with an edge of 40 Å for isolated half-SBUs and 50 Å for couples forming an SBU is used in all cases, respectively, while imposing three-dimensional periodic boundary conditions. All simulations were carried out using GROMACS 5.1[33] with PLUMED 2.2[41].

In the case of isolated half-SBUs in solution, we investigate the structural flexibility of all three isomers. In this context, we sample their conformational space performing WTmetaD simulations using the radius of gyration (Rgyr) as a collective variable (CV). Furthermore, the association of half-SBUs into SBUs was investigated using 2 CVs, namely M-T and M-M. M corresponds to any of the chromium atoms of one metal center and T to any of the terminal carbon atoms of the terephthalate linkers. M-T and M-M are defined as the lowest components of the distances between any M and any T.

Both sets of simulations were performed by depositing Gaussians of initial height 0.598 kcal/mol and width (σ) 0.1 Å every 500 steps (1ps). Isolated half-SBUs simulations were carried out with a bias factor of 10. In simulations studying the association of half-SBUs into SBUs, bias factor is chosen as follows: 30 for MLA-MLA (AA), 20 for MLA-MLB (AB), MLA-MLC (AC), MLB-MLB (BB) and 10 for MLB-MLC (BC), MLC-MLC (CC). The choice of bias factor was dictated by the energy barriers present in each case and these differ between SBUs. Nevertheless, the final free energy estimates are independent of this choice. We note that the same WTmetaD setup was implemented in both the absence and presence of ions in water. Finally, in DMF, the bias factors used were: 50 for AA, 40 for AC, 30 for AB, BB, BC and CC. The overall simulation time in water is 7 μs in the absence and 1 μs in the presence of ions for each one of the 6 combinations of half-SBUs. In DMF, the simulation time is 4 μs for AA, 2.5 μs for AC and 2 μs for the remaining couples of half-SBUs.

Free energy calculations allow us to study the formation of crystal-like and non-crystal-like SBUs from detached half-SBUs. All possible couples of configurational isomers MLA, MLB, MLC are investigated. The SBU dimers (AA, AB, AC, BB, BC, CC) are distinguished into two categories as D_C for crystal-like and D_{NC} for non-crystal-like SBUs, where D indicates one of the aforementioned dimers e.g., AA.

DFT calculations

We further examine the relative stability of the conformational isomers of half-SBU dimers by computing their relative energy at the DFT level. Calculations are conducted in Gaussian 16[42] with the hybrid, gradient-corrected Perdew, Burke and Ernzerhof (PBE0)[43-44] functional for exchange correlation. Single point energy calculations were carried out in the gas phase. We used the 6-31G**[45] basis set for carbon, hydrogen and oxygen and the "Stuttgart RSC 1997"[46] along with its corresponding effective core potential for chromium. The latter were obtained from the EMSL basis set exchange[46-47].

Equilibrium distribution of species

Free energy differences obtained from sampling the conformational landscape of SBUs allow us to compute the equilibrium distribution of SBU conformers in absence and presence of ions. The equilibrium probability of forming crystal-like or non-crystal-like SBUs from any of the six possible half-SBU dimers is estimated from free energy differences under the assumption that half-SBUs can only form SBUs without considering their further assembly into larger structures. It has been observed before that MOF crystallization quickly follows after SBU formation[27]. Two types of dimerization processes are considered:

$$M1 + M2 \rightleftharpoons D_C, \qquad M1 + M2 \rightleftharpoons D_{NC} \quad (1)$$

where M1 and M2 are any two half-SBUs among MLA, MLB and MLC, and D_C and D_{NC} are the crystal-like and non-crystal-like dimers (SBUs). This leads to considering 12 reactions and 15 species (3 half-SBUs and 12 SBUs). Each species is indicated with the index *i*. For each reaction, denoted with index *j*, we consider the free energy of dimerization from a reference state, where half-SBUs are detached, ΔG_j. Convergence of ΔG_j values is reported in Fig. S14-S16, Supplementary Information (SI), section VI. Each reaction is associated with a conversion λ_j. The number of molecules at equilibrium for species *i* $(n_{i,eq})$ is given by:

$$n_{i,eq} = n_{i,0} + v_{ij} \cdot \lambda_j \quad (2)$$

where v_{ij} is the stoichiometric coefficient of species i in reaction j and $n_{i,0}$ is the initial number of molecules of species i. The equilibrium probability of species i is therefore defined as:

$$P_i = \frac{n_{i,eq}}{\sum_i n_{i,eq}} \quad (3)$$

Values of P_i are computed by numerically solving the following system of non-linear equations:

$$\beta \cdot \Delta G_j + \sum_i v_{ij} \cdot log(P_i) = 0, \qquad 1 \le j \le 12 \quad (4)$$

where $\beta \left(\frac{1}{k_B T}\right)$ is the inverse temperature (k_B: Boltzmann's constant). A numerical solution is computed using a trust-region approach with a dogleg step calculation[48-49].

RESULTS

We carried out an extensive analysis of the conformational space of both isolated half-SBU units and all their possible combinations into SBUs. For the sake of clarity, the MIL-101 (Cr) half-SBUs structural isomers are referred to in this work as MLA, MLB, MLC: in metal linker arrangement A (MLA), all linkers are in the same side of the metal center plane; in arrangement B (MLB), two linkers are on one side and one on the other side of an open site; in arrangement C (MLC) two linkers are on one side and one on the other side of an occupied site. Furthermore, we should note that MLA and MLB are also stereo isomers. A representation of their chemical structure is illustrated in Fig. 1[26].

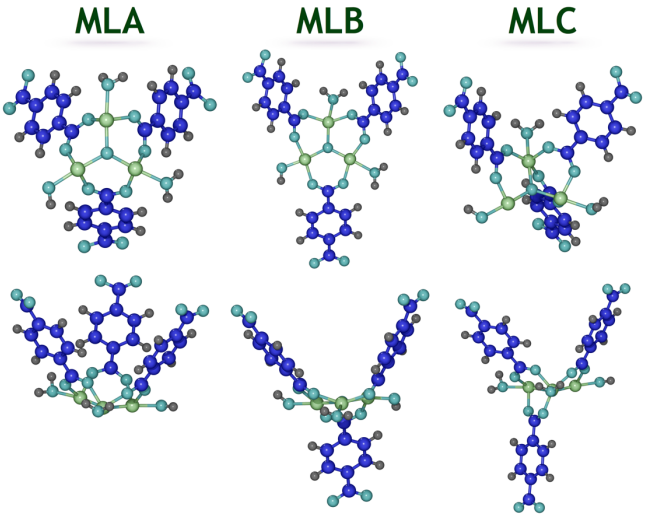

Figure 1. Structural isomers of the MIL-101 (Cr) half-SBU. Color code: Chromium - Lime, Oxygen - Cyan, Hydrogen – Grey, Carbon – Blue. Top: top view, bottom: side view. Considering as a visual reference the plane defined by the Cr atoms in the metal cluster, MLA is characterized by having all terephthalate linkers pointing away from the metal cluster. MLB and MLC instead have only two linker pointing in the same direction. MLB and MLC display a different connectivity between the metal cluster and the linkers, whereby the same two Cr atoms are simultaneously coordinating two linkers. An animated version of this figure is provided as Supplementary Animation.

Well-tempered metadynamics (WTmetaD) simulations were employed to investigate the structural flexibility of half-SBUs, the conformational landscape of SBUs, and the effect of spectator ions and solvent. The most likely half-SBU combinations are identified through computation of the FES of dimerization, which further allow us to evaluate the effect of solvent and spectator ions on the half-SBU interactions and the likelihood of forming crystal-like or non-crystal-like SBUs.

1. Insight into SBU assembly

WTmetaD simulations exploring the conformational space of half-SBU couples were performed at this stage for all combinations of the three half-SBUs – MLA, MLB, and MLC. Our analysis leads to 48 FES and approximately 300 dimer structures in total. The resulting free energy surfaces (FES) exhibit 7 local minima, i.e. (meta) stable states for the system. Low values on both CVs correspond to crystal-like SBUs (minimum 1) and high to detached half-SBUs (state 5). When M-M is low and M-T is high, non-crystal-like SBUs are projected (states 4, 6, 7). Interactions between chromium atoms of a metal center and terminal oxygen atoms of the adjacent terephthalate linker with a planar T-shape represent structures found in the crystal lattice of MIL-101 (Cr). At last, we note that crystal-like SBUs resemble the relative orientation found in the crystal structure, shown in Supporting Information (SI), Fig. S1; hence they are in accordance with experimental observations. All FES are provided in SI, Fig. S2-S8.

Interactions between MLA half-SBUs result in the most stable SBUs. The associated FES, in the case of pure water solution, is presented in Fig. 2. It should be noted that the crystal-like structure in state 2 dominates the equilibrium distribution of species and states 6, 7 correspond to non-crystal-like SBUs with highly positive values that exceed the current scale. Also, a quadruple interaction is observed that corresponds to the same M-T, but lower M-M value than state 2. This is the dominant interaction in DMF, as discussed in section 2a.

In further detail, oxygen atoms of one half-SBU and hydrogen atoms of its counterpart interact in states 3 and 4. Additionally, oxygen and chromium interactions are present in states 1, 2, 6, 7. The nomenclature followed to further describe specific atomic interactions is OMetal: oxygen of the metal center, OTerminal: terminal oxygen of the terephthalate linker. Consequently, we identify the following interactions present, in state 1: [2 OTerminal – 1 Cr], state 2: [2 OTerminal – 2 Cr], state 6: [1 OMetal – 1 Cr] and state 7: [2 OMetal – 2 Cr]. States 1-3 correspond to M-T interactions, while 4, 6 and 7 to M-M. The former stand for all instances that terminal oxygens of a linker that belongs to one half-SBU interact with atoms at the metal center in the other half-SBU. Interactions between the atoms at the metal centers of two different half-SBUs are characterised as M-M. Additional results that support the observed increased stability of MLA-MLA versus other pairs are discussed in the following subsections.

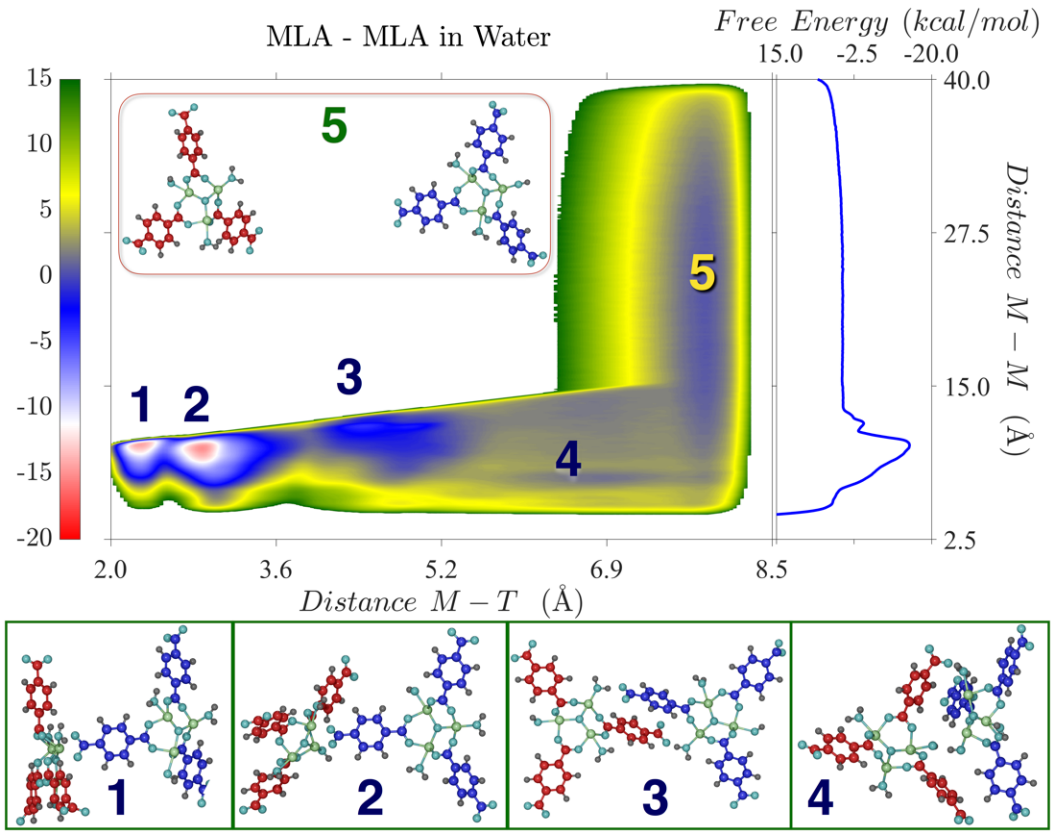

Figure 2. Free energy surface projected on the 2 CVs biased during the simulation of 2 MLA half-SBUs in an aqueous solution. The 4 states of interactions and their respective configurations are shown. State 5 corresponds to detached half-SBUs. The color code for all atoms except from carbon is consistent with Fig. 1. In this representation, carbon atoms are colored blue and red in order to distinguish between different half-SBUs.

1a. Characterization of half-SBU flexibility

We examine the flexibility of isolated half-SBUs in solution through WTmetaD on the radius of gyration (R_{gyr}) of each isomer in solution for 0.2 μs. The resulting free energy is translated to the probability density of each half-SBU structure (Fig. 3a), using the equation below,

$$P(R_{gyr}) = \frac{exp\left(-\beta \cdot F(R_{gyr})\right)}{\int_0^{+\infty} exp\left(-\beta \cdot F(R_{gyr})\right) dR_{gyr}} \quad (5)$$

In MLA, the metal center is easily accessible by another half-SBU. MLB exhibits a bimodal distribution with structures that are similar, but one of the ligands rotate around its axis. MLC shows a configuration with the ligands parallel to each other. The latter observation shows that the most probable configuration for MLC diverges from the orientation found in the crystal lattice, and agrees with the fact that MLC, as emerged from dimerization simulation, is unlikely to produce crystal-like SBUs; especially in the absence of MLA.

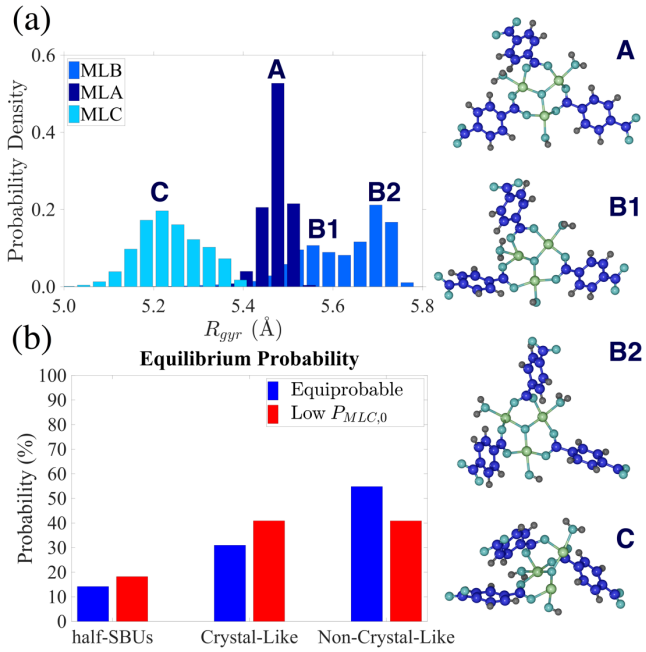

Figure 3. (a) Probability density of isolated half-SBUs in terms of R_{gyr}. The color code is consistent with Fig. 1. All structures refer to (a). (b) Equilibrium distribution of species in absence of ions. Blue: Equiprobable initial distribution of half-SBUs, red: low initial concentration for MLC.

1b. MLA-MLA SBU energies

Following the analysis of the FES conformational landscape, we have conducted single point energy calculations on the AA SBUs in the gas phase. A qualitative agreement with estimates from the classical force field is observed. Therefore, we report that the rank of the structures in terms of energy stays the same as at a higher order of theory. Nevertheless, the potential energy difference (ΔE) is larger at the higher level of theory. The reference structure for these calculations is state 2, as it is, the most stable. All estimates from DFT calculations are provided in table S1, Supplementary Information (SI), section IV.

1c. Equilibrium probability of crystal-like vs non-crystal-like SBUs

The probabilities of different species being present at equilibrium were calculated to provide an estimate for the likelihood of forming crystal-like (C) vs non-crystal-like (NC) SBUs starting from an initial distribution of half-SBUs. The analysis was conducted for the simulations in water and DMF to compare the effect of ions on the population of dominating structures at equilibrium, see section 2a.

The free energy difference for the formation of any of the SBU conformational isomers has been computed considering state 5, i.e. the two detached half-SBUs (see Fig. 1), as a reference.

In order to consider the uncertainty of ΔG on the calculation of the equilibrium distribution of species, we consider two limiting cases, i.e. "strong" and "weak", for the formation of the AA (C) SBU. This SBU exhibits the largest standard deviation in the estimate of the ΔG. The ΔG for each case is provided below:

$$\Delta G_{STRONG} = -|\Delta G_{MEAN} - \sigma| \quad (6a)$$

$$\Delta G_{WEAK} = -|\Delta G_{MEAN} + \sigma| \quad (6b)$$

where σ is the standard deviation and ΔG_{MEAN} is the time-weighted average of ΔG.

We investigate two conditions for the initial distribution of half-SBUs: (1) Equiprobable, (2) $P_{MLA,0} = 45\%, P_{MLB,0} = 45\%, P_{MLC,0} = 10\%$ (Low MLC). The reason for the latter is that the energy barrier is larger in the formation process of MLC than in MLA, MLB[26]. An Equiprobable initial distribution results in ~ 30% probability of formation of crystal-like SBUs, which is increased to ~ 40% when the initial probability of MLC is lower than MLA and MLB[26]. Detached half-SBUs have a probability of ~ 15% and 18% at equilibrium for (1) and (2) respectively. The latter follows after an appreciable decrease in probability of non-crystal-like SBUs (~ 40%) in (2) in contrast to (1) (~ 55%). The resulting probability distributions, considering ΔG_{MEAN} in the calculations, are shown in Fig. 4b. The equilibrium probabilities of all SBUs are available in SI Fig. S9-S13.

2. Effect of Solvents and spectator ions

The presence of spectator ions and choice of solvent change the FES of dimerization impacts the probability of formation of crystal-/non-crystal-like structures.

2a. Evaluation of solvent effects

We investigate the impact of a solvent different than water on the half-SBU association process. DMF is frequently used in MOF synthesis[28, 50-51]. Compared with those obtained in water, SBUs are much more stable and compact in DMF: the values for the ΔG (in kcal/mol) are -115 for AA, -55 for AB, AC, -35 for CC and -20 for the rest.

In most cases, only one SBU state dominates the FES. The configurations that corresponds to this state display 4 OMetal – Cr interactions and the half-SBUs are parallel to each other (Fig. 4a) or slightly bent (Fig. 4b). The former is the most stable structure in DMF and it has been formed in water as well, however it is not as stable in the latter. Moreover, AA again dominates all SBUs from a free energy of association standpoint. Another interesting structure that is found in DMF presents the terminal oxygen atoms from 2 linkers of one half-SBU bound to all 3 Cr atoms of its counterpart (Fig. 4c). It should be noted that $\pi - \pi$ stacking of the benzene rings characterizes these structures. All of the aforementioned conformers are provided along with the corresponding FES in Fig. 4.

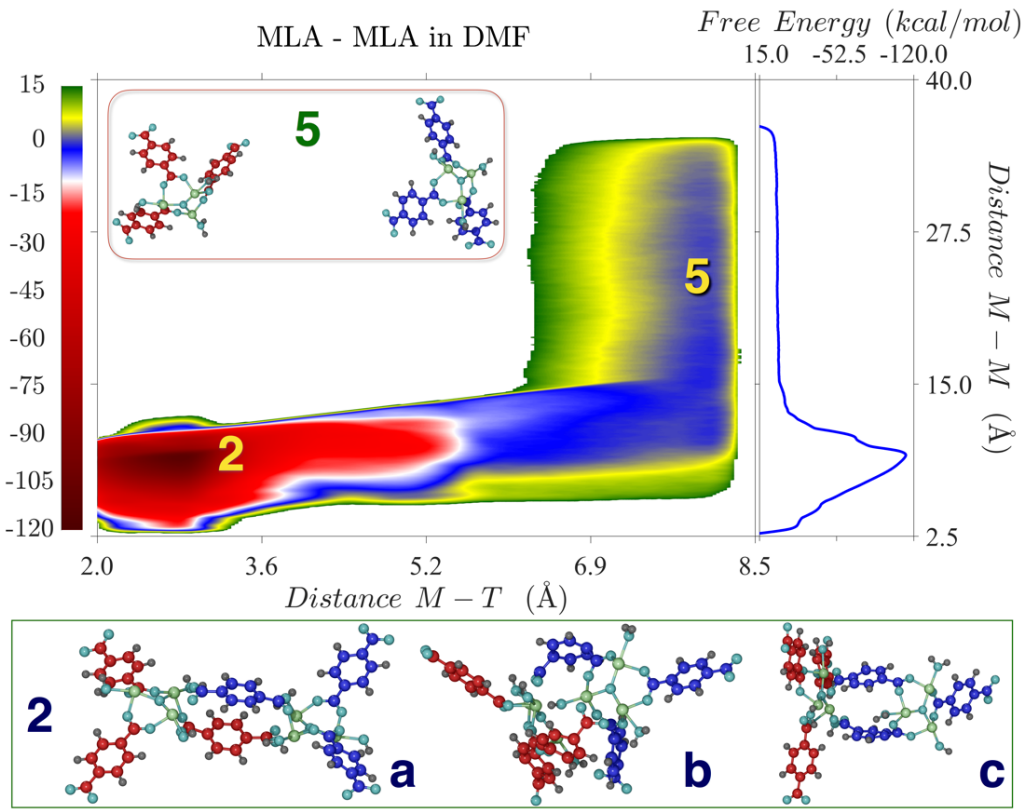

Figure 4. Free energy surface projected on the 2 CVs biased during the simulation of 2 MLA half-SBUs in DMF. Configurations present in states 2 and 5 are shown. State 5 corresponds to detached half-SBUs. The color code is consistent with Fig 2. The free energy scale has been extended to with respect to previous cases.

2b. Impact of ions on SBU configurational landscape

The same approach is followed after the introduction of spectator ions to the system of half-SBUs in water, both explicitly represented. Ionic species are $Na^+$and F^- at concentrations of 0.025, 0.125, 0.25, 0.5, 0.75, and1 M.

An analysis of the structures reveals that ions tend to bind the metal centers, and to promote M-M interactions in small concentrations (<0.125 M). In order to characterise the binding of half-SBUs in the presence of ions, we discuss AA as it is the most energetically favourable SBU. A small concentration of ions (0.025M) results in energetics and structures that are comparable to those obtained in absence of ions. Nevertheless, the probability of crystal-like SBUs is marginally greater because fewer half-SBUs are unbound at equilibrium. A further increase (> 0.125M and < 0.5 M) renders crystal-like structures improbable because states 6, 7 corresponding to M-M interactions emerge and dominate the FES, see also SI section III, Fig. S3-S8. Fluoride anions interact with the metal centers promoting non-crystal-like SBUs at this stage. Two F^- interact with two hydrogen and two Cr atoms in states 6 and 7 respectively. Similar behaviour is exhibited for a concentration of ions equal to 0.25M, where state 6 dominates, while states 1, 2 and 7 are improbable ($\Delta G_{5\rightarrow 1,2} < +15$ kcal/mol, see Fig 5). Additional interactions between the metal centers are observed for 0.5M, where F^- linked to the metal centers interact with Na^+ forming salt bridges between the half-SBUs (state 4U, see Fig. 5).

Beyond 0.5 M, ions have a two-fold effect. On the one hand ions decrease the total amount of SBUs formed, on the other hand however the introduction of salt bridges favours the stabilization of crystal-like SBUs. This behaviour is apparent through states 5B, 5M, 5T (Fig. 5) at 1M. The FES for AA SBUs in water at ionic concentrations 0.025M, 0.5M and 1M along with the corresponding structures are available in Fig. 5, while the intermediate concentrations are available in SI, section III, Fig. S3.

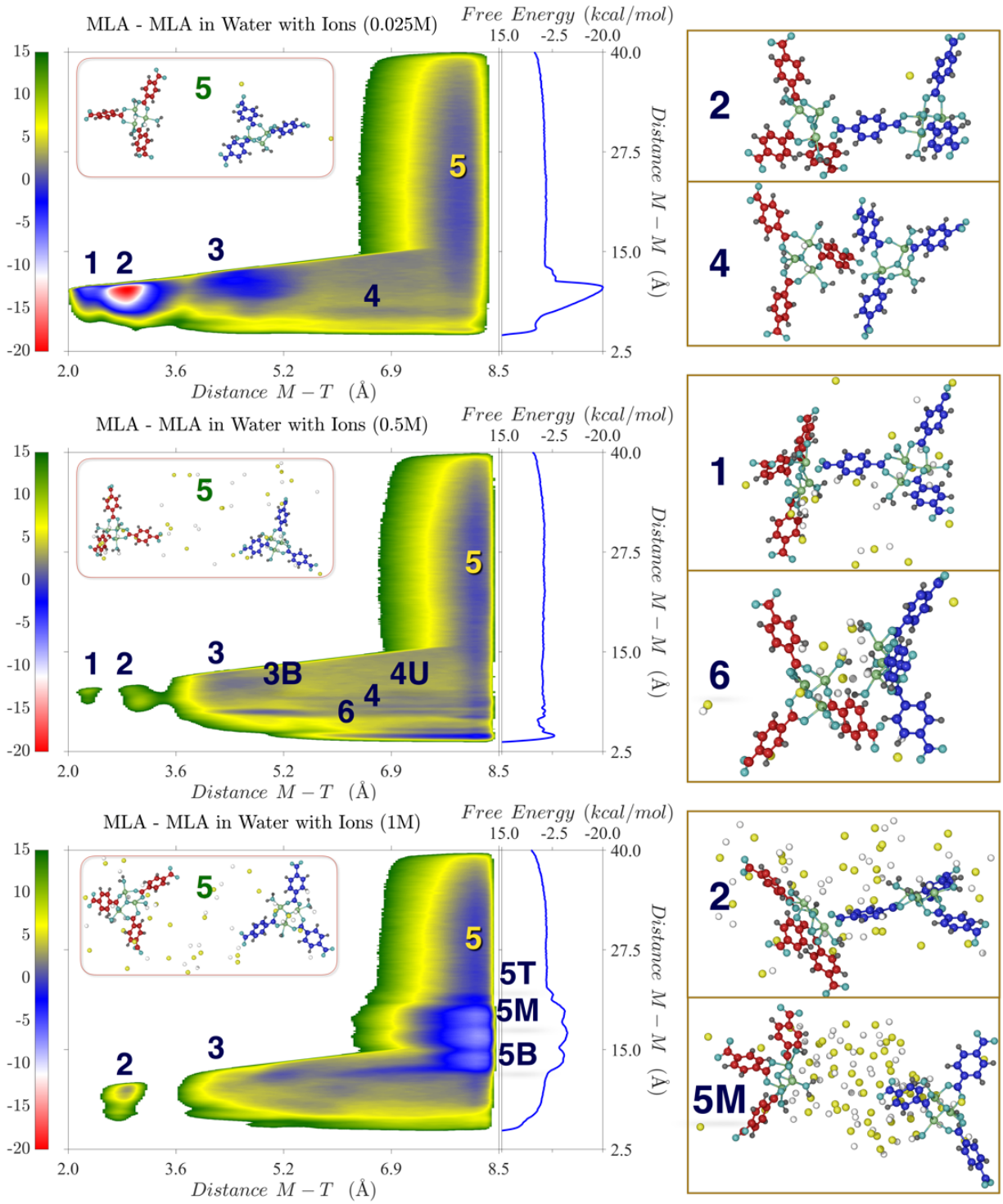

Figure 5. Free Energy Surfaces of MLA – MLA interactions in the presence of ions in water. The structure of the dominant non-crystal-like state is shown for every case (bottom configuration at the side of each FES) along with the crystal-like conformer (top configuration at the side of each FES). Reference state (5) is also shown for each concentration of ions. The color code is consistent with Fig. 2.

2c. Impact of spectator ions on the equilibrium distribution of species

Following the procedure outlined in the previous paragraphs, the equilibrium probability of detached half-SBUs, crystal like SBUs and non-crystal-like SBUs has been computed for all the concentrations of ions investigated. The resulting probability distributions are available in SI, section V, Fig. S9-S13. Equilibrium probability distributions allow us to assess the effect of ionic strength on the relative abundance of conformational isomers of SBUs. In Fig. 6 we observe that the probability of crystal-like SBUs presents a non-monotonous trend as a function of the ionic strength. In particular, we see that crystal-like SBUs are observed in significant amounts at ionic strengths < 0.125M or > 0.5M, while their contribution to the overall population of species formed by dimerization of half-SBUs is negligible at intermediate values of the ionic strength.

This behaviour can be rationalized by looking at the interactions between ions and SBUs. At low concentrations, the species distribution is akin to the one obtained in absence of ions and discussed in detail in Fig. 4b. Increasing the concentration of ions however, long lived interactions between counter ions and metal clusters are observed. These interactions hinder the occurrence of the M-T associations seen in crystal-like SBUs and lead to a negligible probability of observing crystal-like SBU configurations, like states 1 and 2 in the FES reported in Fig. 4b. In these intermediate conditions non-crystal-like SBUs, characterized by specific interactions (states 4, 6 and 7) are favoured. Nevertheless, when the ionic concentration exceeds the threshold of 0.5M, salt bridges are formed between half-SBUs. Such ion-mediated interactions hinder rotation of the linkers and promote crystal-like SBU configurations.

These findings suggest a complex role played by ions during MOF synthesis:

- At low ion concentrations (0 to 0.2 M in our simulations), unbound MLA half-SBUs are very improbable, therefore even if (C) SBUs are formed, their growth is likely to propagate through the addition of MLB or MLC. This makes it more prone to introduce defects in the crystal structure.
- At slightly higher concentrations, 0.2 - 0.5 M in our simulations - spectator ions inhibit the formation of C-SBUs. Above that threshold instead, the formation of salt bridges between with half-SBUs has the opposite effect, favouring the formation of crystal-like units.

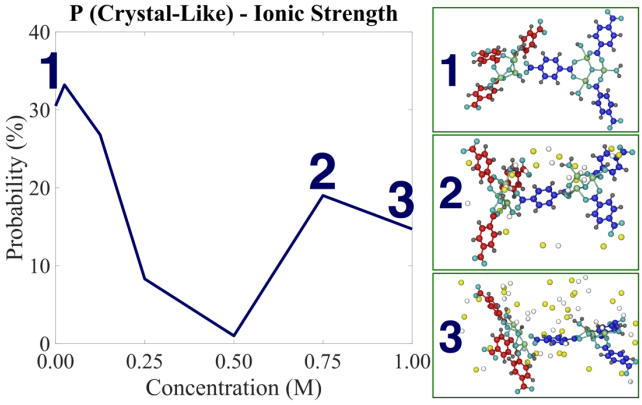

Figure 6. Probability of formation of crystal-like SBUs at equilibrium with increasing concentration of ions. The configurations present at different instances correspond to the AA SBU and the color code is consistent with Fig. 2.

DISCUSSION AND CONCLUSIONS

In this work, we investigate the early stages of the MIL-101 (Cr) nucleation by studying the bonding behaviour of its building units. At first, we assess the flexibility of three structural isomers of the half-SBUs. This analysis shows how half-SBUs differ on the accessibility of the metal center from an adjacent terephthalate linker. In this context, MLA has the largest accessible volume, MLB shows two favourable structures with a certain degree of steric hindrance and MLC is highly probable to exist with the linkers parallel to each other; hence it is more likely to be a source of defects where the linkers are found in such geometry.

The interactions between half-SBUs highlight the different ways in which the MIL-101 (Cr) lattice can be formed, which involve crystal-like and non-crystal-like SBUs whose relative interaction strength is expressed in terms of formation probability from detached half-SBUs. More precisely, the propensity of forming SBUs is evaluated for all six possible combinations of half-SBU couples.

The simulations reveal a remarkable conformational ensemble of 300 structures after extensive sampling of microsecond long WTmetaD simulations for the association of half-SBUs to SBUs in different solvents and varying ionic concentration. In aqueous solution, the most stable SBU is produced by AA with a ΔG of formation of -15 kcal/mol, while for the other combinations, ΔG is ~ -5 kcal/mol. The stability of AA could be due to MLA having the largest accessible volume, hence promoting binding of terminal oxygen atoms from adjacent terephthalate linkers to its metal center. This is further quantified by the equilibrium distribution of species, where crystal-like SBUs originating from MLA are present with a probability 30 - 40% depending on the different starting conditions of the initial distribution of half-SBUs.

Counterion effects are assessed through the addition of increasing amounts of Na^+ and F^-. Fluoride anions tend to cluster around the metal centers of the half-SBUs and in this context, a very small increase in concentration of NaF has only weak effect on the probability of forming crystal-like SBUs, and gradually decreases as the concentration of ions increases up to ~ 0.5M. At higher ionic concentrations (>0.5M) salt bridges are formed reducing the rotational freedom of the terephthalate linkers and reducing the probability of defects. Higher ion concentrations further diminish the interactions between half-SBUs due to formation of ionic clusters.

Solvent effects were evaluated by introducing DMF as a solvent instead of water. SBUs are much more stable and compact in DMF as the values for the ΔG of transition from the reference state are appreciably lower than in water, regardless of the presence of ions. The dominating structure corresponds to half-SBUs aligning with each other.

In closing, this study documents in detail how the complexity of the configurational landscape controls materials synthesis. Solvents can be used to direct speciation towards desired isomers, as shown in the case of DMF vs water. The implications are that both thermodynamic and kinetic factors are at play, indicating how solvent mixture can be used to control self-assembly. Similarly, spectator ions and solution ionic strength can also be used to selectively shut down or open up pathways and control defect concentrations. Given that these effects arise from both enthalpic and entropic drivers, it is not a priori obvious which will dominate based on simple intuition alone. The identification of these factors demands full knowledge of the free energy landscapes and their dependence on synthesis conditions. Modern molecular simulations methods can be used to discriminate these critical drivers and provide a hypothesis-based approach to synthesis that departs from traditional Edisonian practices.

ASSOCIATED CONTENT

Supporting Information

The Supporting Information is available free of charge on the ACS Publications website.

Supplementary information (SI) linked with the main article (PDF)
Half-SBUs atomic coordinate files (XYZ)
Half-SBUs topology files (ITP)
Half-SBUs movie (MPG)

AUTHOR INFORMATION

Corresponding Author

*m.salvalaglio@ucl.ac.uk

*Vanda.Glezakou@pnnl.gov

Notes

The authors declare no competing financial interest.

ACKNOWLEDGMENTS

The work described in this publication was performed by Pacific Northwest National Laboratory, which is operated by Battelle for the United States Department of Energy under Contract DE-AC05-76RL01830. The authors acknowledge the use of the UCL Legion High Performance Computing Facility (Legion @ UCL), and associated support services, in the completion of this work. This research used resources of the National Energy Research Scientific Computing Center, a DOE Office of Science User Facility supported by the Office of Science of the U.S. Department of Energy under Contract No. DE- SUPPLEMENTARY MATERIAL AC02-05CH11231.

REFERENCES

1. Yu, J.; Xie, L.-H.; Li, J.-R.; Ma, Y.; Seminario, J. M.; Balbuena, P. B., CO_2 Capture and Separations Using MOFs: Computational and Experimental Studies. *Chem. Rev.* **2017,** *117* (14), 9674-9754.
2. Trickett, C. A.; Helal, A.; Al-Maythalony, B. A.; Yamani, Z. H.; Cordova, K. E.; Yaghi, O. M., The chemistry of metal–organic frameworks for CO_2 capture, regeneration and conversion. *Nat. Rev. Mater.* **2017,** *2* (8), 17045-17045.
3. Fracaroli, A. M.; Furukawa, H.; Suzuki, M.; Dodd, M.; Okajima, S.; Gandara, F.; Reimer, J. A.; Yaghi, O. M., Metal-organic frameworks with precisely designed interior for carbon dioxide capture in the presence of water. *J. Am. Chem. Soc.* **2014,** *136* (25), 8863-6.
4. Duren, T.; Sarkisov, L.; Yaghi, O. M.; Snurr, R. Q., Design of new materials for methane storage. *Langmuir* **2004,** *20* (7), 2683-9.
5. Jiang, J.; Furukawa, H.; Zhang, Y. B.; Yaghi, O. M., High Methane Storage Working Capacity in Metal-Organic Frameworks with Acrylate Links. *J. Am. Chem. Soc.* **2016,** *138* (32), 10244-51.
6. Lee, J.; Farha, O. K.; Roberts, J.; Scheidt, K. A.; Nguyen, S. T.; Hupp, J. T., Metal-organic framework materials as catalysts. *Chem. Soc. Rev.* **2009,** *38* (5), 1450-1459.
7. Park, H. D.; Dinca, M.; Roman-Leshkov, Y., Continuous-Flow Production of Succinic Anhydrides via Catalytic beta-Lactone Carbonylation by Co(CO)4 subsetCr-MIL-101. *J. Am. Chem. Soc.* **2018**.
8. Horcajada, P.; Gref, R.; Baati, T.; Allan, P. K.; Maurin, G.; Couvreur, P., Metal - Organic Frameworks in Biomedicine. *Chem. Rev.* **2012,** *112* (2), 1232-1268.
9. Horcajada, P.; Chalati, T.; Serre, C.; Gillet, B.; Sebrie, C.; Baati, T.; Eubank, J. F.; Heurtaux, D.; Clayette, P.; Kreuz, C.; Chang, J. S.; Hwang, Y. K.; Marsaud, V.; Bories, P. N.; Cynober, L.; Gil, S.; Férey, G.; Couvreur, P.; Gref, R., Porous metal-organic-framework nanoscale carriers as a potential platform for drug delivery and imaging. *Nat. Mater.* **2010,** *9* (2), 172-178.
10. Van Vleet, M. J.; Weng, T.; Li, X.; Schmidt, J. R., In Situ, Time-Resolved, and Mechanistic Studies of Metal-Organic Framework Nucleation and Growth. *Chem. Rev.* **2018,** *118* (7), 3681-3721.
11. Li, J. R.; Sculley, J.; Zhou, H. C., Metal-organic frameworks for separations. *Chem Rev* **2012,** *112* (2), 869-932.
12. Fathieh, F.; Kalmutzki, M. J.; Kapustin, E. A.; Waller, P. J.; Yang, J.; Yaghi, O. M., Practical water production from desert air. *Sci Adv* **2018,** *4* (6), eaat3198.
13. Howarth, A. J.; Liu, Y.; Li, P.; Li, Z.; Wang, T. C.; Hupp, J. T.; Farha, O. K., Chemical, thermal and mechanical stabilities of metal–organic frameworks. *Nat. Rev. Mater.* **2016,** (15018).
14. Howarth, A. J.; Peters, A. W.; Vermeulen, N. A.; Wang, T. C.; Hupp, J. T.; Farha, O. K., Best Practices for the Synthesis, Activation, and Characterization of Metal–Organic Frameworks. *Chem. Mater.* **2017,** *29* (1), 26-39.
15. Taddei, M., When defects turn into virtues : The curious case of zirconium-based metal-organic frameworks. *Coord. Chem. Rev.* **2017,** *343*, 1-24.
16. Gutov, O. V.; Hevia, M. G.; Escudero-Adán, E. C.; Shafir, A., Metal-Organic Framework (MOF) Defects under Control: Insights into the Missing Linker Sites and Their Implication in the Reactivity of Zirconium-Based Frameworks. *Inorg. Chem.* **2015,** *54* (17), 8396-8400.
17. Férey, G.; Mellot-Draznieks, C.; Serre, C.; Millange, F.; Dutour, J.; Surblé, S.; Margiolaki, I.; Ferey, G., A chromium terephthalate-based solid with unusually large pore volumes and surface area. *Science* **2005,** *309*, 2040-2042.
18. Loiseau, T.; Férey, G., Crystalline oxyfluorinated open-framework compounds: Silicates, metal phosphates, metal fluorides and metal-organic frameworks (MOF). *J. Fluor. Chem.* **2007,** *128* (4), 413-422.
19. Leng, K.; Sun, Y.; Li, X.; Sun, S.; Xu, W., Rapid Synthesis of Metal-Organic Frameworks MIL-101(Cr) Without the Addition of Solvent and Hydrofluoric Acid. *Cryst. Growth Des.* **2016,** *16* (3), 1168-1171.
20. Mishra, S.; Daniele, S., Metal-organic derivatives with fluorinated ligands as precursors for inorganic nanomaterials. *Chem. Rev.* **2015,** *115* (16), 8379-8448.
21. Bromberg, L.; Diao, Y.; Wu, H.; Speakman, S. A.; Hatton, T. A., Chromium (III) terephthalate metal organic framework (MIL-101): HF-free synthesis, structure, polyoxometalate composites, and catalytic properties. *Chem. Mater.* **2012,** *24* (9), 1664-1675.
22. Yang, J.; Zhao, Q.; Li, J.; Dong, J., Synthesis of metal-organic framework MIL-101 in TMAOH-$Cr(NO_3)_3$-H_2BDC-H_2O and its hydrogen-storage behavior. *Microporous Mesoporous Mater.* **2010,** *130* (1-3), 174-179.
23. Rallapalli, P.; Raj, M. C.; Senthilkumar, S.; Somani, R. S.; Bajaj, H. C., HF-Free Synthesis of MIL-101(Cr) and Its Hydrogen Adsorption Studies. *Environ. Prog. Sustain. Energy* **2016,** *35* (2), 461-468.
24. Liang, Z.; Marshall, M.; Ng, C. H.; Chaffee, A. L., Comparison of conventional and HF-free-synthesized MIL-101 for CO_2 adsorption separation and their water stabilities. *Energy and Fuels* **2013,** *27* (12), 7612-7618.
25. Low, J. J.; Jakubczak, P.; Abrahamian, J. F.; Faheem, S. A.; Willis, R. R., Virtual High Throughput Screening Confirmed Experimentally: Porous Coordination Polymer Hydration. *J. Am. Chem. Soc.* **2009,** *131* (5), 15834-15842.
26. Cantu, D. C.; McGrail, B. P.; Glezakou, V. A., Formation mechanism of the secondary building unit in a chromium terephthalate metal-organic framework. *Chem. Mater.* **2014,** *26* (22), 6401-6409.
27. Férey, G.; Haouas, M.; Loiseau, T.; Taulelle, F., Nanoporous solids: How do they form? An in situ approach. *Chem. Mater.* **2014,** *26* (1), 299-309.
28. Goesten, M. G.; Stavitski, E.; Juan-Alcañiz, J.; Martiñez-Joaristi, A.; Petukhov, A. V.; Kapteijn, F.; Gascon, J., Small-angle X-ray scattering documents the growth of metal-organic frameworks. *Catal. Today* **2013,** *205*, 120-127.
29. Embrechts, H.; Kriesten, M.; Hoffmann, K.; Peukert, W.; Hartmann, M.; Distaso, M., Elucidation of the Formation Mechanism of Metal-Organic Frameworks via in-Situ Raman and FTIR Spectroscopy under Solvothermal Conditions. *J. Phys. Chem. C* **2018**.
30. Humphrey, W.; Dalke, A.; Schulten, K., VMD - Visual Molecular Dynamics. *J. Mol. Graph.* **1996,** *14*, 33-38.

31. Jorgensen, W. L.; Tirado-Rives, J., The OPLS Potential Functions for Proteins. Energy Minimizations for Crystals of Cyclic Peptides and Crambin. *J. Am. Chem. Soc.* **1988,** *110* (6), 1657-1666.

32. Jorgensen, W. L.; Chandrasekhar, J.; Madura, J. D.; Impey, R. W.; Klein, M. L., Comparison of simple potential functions for simulating liquid water. *J. Chem. Phys.* **1983,** *79* (2), 926-926.

33. Abraham, M. J.; Murtola, T.; Schulz, R.; Páll, S.; Smith, J. C.; Hess, B.; Lindahl, E., GROMACS: High performance molecular simulations through multi-level parallelism from laptops to supercomputers. *SoftwareX* **2015,** *1-2*, 19-25.

34. Caleman, C.; Van Maaren, P. J.; Hong, M.; Hub, J. S.; Costa, L. T.; Van Der Spoel, D., Force field benchmark of organic liquids: Density, enthalpy of vaporization, heat capacities, surface tension, isothermal compressibility, volumetric expansion coefficient, and dielectric constant. *J. Chem. Theory Comput.* **2012,** *8* (1), 61-74.

35. van der Spoel, D.; van Maaren, P. J.; Caleman, C., GROMACS molecule & liquid database. *Bioinformatics* **2012,** *28* (5), 752-753.

36. Barducci, A.; Bussi, G.; Parrinello, M., Well-tempered metadynamics: A smoothly converging and tunable free-energy method. *Phys. Rev. Lett.* **2008,** *100* (2), 1-4.

37. Bussi, G.; Donadio, D.; Parrinello, M., Canonical sampling through velocity rescaling. *J. Chem. Phys.* **2007,** *126* (1).

38. Berendsen, H. J. C.; Postma, J. P. M.; van Gunsteren, W. F.; DiNola, A.; Haak, J. R., Molecular dynamics with coupling to an external bath. *J. Chem. Phys.* **1984,** *81* (1984), 3684-3690.

39. Darden, T.; York, D.; Pedersen, L., Particle mesh Ewald: An N·log(N) method for Ewald sums in large systems. *J. Chem. Phys.* **1993,** *98* (12), 10089-10092.

40. Hess, B.; Bekker, H.; Berendsen, H. J. C.; Fraaije, J. G. E. M., LINCS: A linear constraint solver for molecular simulations. *J. Comput. Chem.* **1997,** *18* (12), 1463-1472.

41. Tribello, G. A.; Bonomi, M.; Branduardi, D.; Camilloni, C.; Bussi, G., PLUMED 2: New feathers for an old bird. *Comput. Phys. Commun.* **2014,** *185* (2), 604-613.

42. Frisch, M. J.; Trucks, G. W.; Schlegel, H. B.; Scuseria, G. E.; Robb, M. A.; Cheeseman, J. R.; Scalmani, G.; Barone, V.; Petersson, G. A.; Nakatsuji, H.; Li, X.; Caricato, M.; Marenich, A.; Bloino, J.; Janesko, B. G.; Gomperts, R.; Mennucci, B.; Hratchian, H. P.; Ortiz, J. V.; Izmaylov, A. F.; Sonnenberg, J. L.; Williams-Young, D.; Ding, F.; Lipparini, F.; Egidi, F.; Goings, J.; Peng, B.; Petrone, A.; Henderson, T.; Ranasinghe, D.; Zakrzewski, V. G.; Gao, J.; Rega, N.; Zheng, G.; Liang, W.; Hada, M.; Ehara, M.; Toyota, K.; Fukuda, R.; Hasegawa, J.; Ishida, M.; Nakajima, T.; Honda, Y.; Kitao, O.; Nakai, H.; Vreven, T.; Throssell, K.; Montgomery, J. A., Jr.; Peralta, J. E.; Ogliaro, F.; Bearpark, M.; Heyd, J. J.; Brothers, E.; Kudin, K. N.; Staroverov, V. N.; Keith, T.; Kobayashi, R.; Normand, J.; Raghavachari, K.; Rendell, A.; Burant, J. C.; Iyengar, S. S.; Tomasi, J.; Cossi, M.; Millam, J. M.; Klene, M.; Adamo, C.; Cammi, R.; Ochterski, J. W.; Martin, R. L.; Morokuma, K.; Farkas, O.; Foresman, J. B.; Fox, D. J. *Gaussian 16, Revision A.03*, Gaussian Inc.: Wallingford CT, 2016.

43. Perdew, J. P.; Burke, K.; Ernzerhof, M., Generalized gradient approximation made simple. *Phys. Rev. Lett.* **1996,** *77* (18), 3865-3868.

44. Adamo, C.; Barone, V., Toward reliable density functional methods without adjustable parameters: The PBE0 model. *J. Chem. Phys.* **1999,** *110* (13), 6158-6170.

45. Hariharan, P. C.; Pople, J. A., The influence of polarization functions on molecular orbital hydrogenation energies. *Theor. Chim. Acta* **1973,** *28* (3), 213-222.

46. Feller, D., The role of databases in support of computational chemistry calculations. *J. Comput. Chem.* **1996,** *17* (13), 1571-1586.

47. Schuchardt, K. L.; Didier, B. T.; Elsethagen, T.; Sun, L.; Gurumoorthi, V.; Chase, J.; Li, J.; Windus, T. L., Basis set exchange: A community database for computational sciences. *J. Chem. Inf. Model.* **2007,** *47* (3), 1045-1052.

48. Dennis, J. E.; Schnabel, R. B., *Numerical Methods for Unconstrained Optimization and Nonlinear Equations*. Society for Industrial and Applied Mathematics: 1996.

49. Powell, M. J. D., *Numerical methods for nonlinear algebraic equations*. Gordon and Breach Science Publishers: 1970.

50. Goesten, M. G.; Magusin, P. C. M. M.; Pidko, E. A.; Mezari, B.; Hensen, E. J. M.; Kapteijn, F.; Gascon, J., Molecular promoting of aluminum metal-organic framework topology MIL-101 by N, N-dimethylformamide. *Inorg. Chem.* **2014,** *53* (2), 882-887.

51. Stylianou, K. C.; Heck, R.; Chong, S. Y.; Bacsa, J.; Jones, J. T. a.; Khimyak, Y. Z.; Bradshaw, D.; Rosseinsky, M. J., A Guest-Responsive Fluorescent 3D Microporous Metal-Organic Framework Derived from a Long-Lifetime Pyrene Core. *J. Am. Chem. Soc.* **2010,** *132* (8), 4119-4130.

Graphic entry for the Table of Contents (TOC)